ELSEVIER

Journal of Fluids and Structures 25 (2009) 867–888

JOURNAL OF FLUIDS AND STRUCTURES

www.elsevier.com/locate/jfs

The interaction of a bluff body with a vortex wake

D.J.J. Leclercq, C.J. Doolan*

School of Mechanical Engineering, The University of Adelaide, Adelaide, SA 5005, Australia

Received 11 December 2007; accepted 5 March 2009
Available online 25 April 2009

Abstract

A theoretical, experimental and numerical study is presented of the interaction of a vortex–wake created by an upstream blade with a downstream prismatic block. The aim of the study is to investigate the fundamentals of force and noise generation for this type of flow and explain how inter-object spacing affects the far-field noise level. A theoretical model, based on a compact form of Curle's formulation, is developed and shows that acoustically constructive or destructive interference is determined by the amplitude and phase of the forces on each object. Experimental and two-dimensional, unsteady numerical results of the vortex–wake interaction case are presented for several blade–block separation distances. Using a combination of experimental and numerical data, the theoretical model is able to explain observed variations in far-field noise level with blade–block separation distance. The numerical model accurately predicts the phase relationship between the unsteady forces on each object.

Keywords: Vortex–wake interaction; Curle's formulation; Noise

1. Introduction

The buffeting of bluff bodies is of fundamental concern to those involved in the aerodynamics of buildings, bridges, automobiles and aircraft. The fluctuating loads are the cause of fatigue loading, undesirable structural movement and annoying radiated noise that needs to be understood and controlled for better industrial design and improved public health through the provision of quieter living areas. This paper is concerned with the particular case of noise caused by the interaction of a vortex dominated wake (or vortex wake) generated by an upstream body with another, prismatic object.

The arrangement of tandem, in-line cylinders is the most investigated form of wake interaction to be found in the literature. Zdravkovich (1987) provides an excellent review of the early work in this area. Examples of more recent studies include the work performed by Papaioannou et al. (2006), who simulated the three-dimensional laminar and early turbulent flow about tandem in-line cylinders. Meneghini et al. (2001) also performed a two-dimensional study for laminar flow about tandem cylinders, while Fitzpatrick (2003) studied the flow and noise generated by turbulent flow over tandem cylinders. As originally classified by Zdravkovich (1987), tandem cylinder flows are considered as a problem in wake interference. The separation between the cylinders sets the type of wake interaction. Essentially, when the cylinders are close to one another, vortex shedding from the upstream cylinder has been found to be suppressed.

*Corresponding author. Tel.: +61 8 8303 8261; fax: +61 8 8303 4367.
E-mail address: con.doolan@mecheng.adelaide.edu.au (C.J. Doolan).
URL: http://www.mecheng.adelaide.edu.au/~cdoolan/ (C.J. Doolan).

0889-9746/$ - see front matter © 2009 Elsevier Ltd. All rights reserved.
doi:10.1016/j.jfluidstructs.2009.02.005

As the cylinder spacing is increased, a variety of flow modes are encountered (sometimes with hysteresis effects), with upstream shear layer reattachment occurring first on the downstream cylinder, followed by the re-estabishment of vortex shedding behind the upstream cylinder. Once this occurs, the impingement of the wake on the downstream body creates high amplitude unsteady forces and intense radiated noise. Hydrodynamic feedback between the cylinders synchronises their vortex shedding frequencies until the separation distance becomes very large. Most studies have been performed at relatively low Reynolds number, however; recent experimental and numerical work at high Reynolds number has been reported by Khorrami et al. (2007). While more complicated than the lower Reynolds number studies, this work confirms that similar flow physics control the interaction in this flow regime as does related work (Jacob et al., 2005) that examines the interaction of a turbulent cylinder wake with an airfoil.

Relatively recent aerodynamic investigations of vortex–wake or tandem bluff (sharp-edged) body interactions include the work by Devarakonda and Humphrey (1996), who show that significant changes in unsteady forces and flow field are observed with the addition of a second prism. Bull et al. (1996) and Blazewicz et al. (2007) have conducted a series of flow and acoustic experiments for interacting tandem plates at low to moderate Reynolds number. These experiments show similar behaviour to interacting circular cylinders in that there exists flow regimes where the vortex shedding from the upstream plate is either suppressed or supported, depending on the separation distance between the plates. Once the upstream plate sheds coherent vortex structures, the unsteady force amplitude increases dramatically on the downstream plate and the observed sound pressure level also increases. This was attributed (Blazewicz et al., 2007) to the vortex interaction at the leading edge of the downstream plate.

Hangan and Vickery (1999) develop an empirical buffeting load model for tandem bluff bodies from detailed experimental results. The results show significant variation in aerodynamic forces based on separation distance. This work was extended for two- and three-dimensional bluff bodies placed in boundary layers (Havel et al., 2001). Obi and Tokai (2006) investigated the flow between two rounded thick plates at fixed separation distance (set at twice the plate thickness) using particle image velocimetry and unsteady surface pressure measurements. The aim of this work was to provide data for validating numerical methods, however, results showed strong turbulence between the bodies that was attributed to vortex shedding by the upstream plate.

Applied aeroacoustic studies for the vortex–wake interaction for sharp edged bluff bodies are relatively rare in the literature. Johnson and Loehrke (1984) measured the noise generated by tandem plates in an effective free-field. They found that acoustic feedback affected flow and noise only when the wake between the plates was laminar. Once the Reynolds number was increased so that turbulent flow existed in the wake, acoustic feedback effects were not noticed and variations in sound level with plate separation were thought to be due to sources on each plate that reinforced or cancelled each other, depending on their phase difference.

Stoneman et al. (1988) performed a study of tandem plates in a duct. The duct acoustic modes were excited by the hydrodynamic field and a strong coupling between the acoustic and hydrodynamic fields was observed. In the current work, the experiments do not excite any acoustic duct modes, so while the results of Stoneman et al. (1988) are important, they are not completely representative of wake interference in an acoustic free-field. Of more relevance to the present paper is the work on circular saw-blade noise by Martin and Bies (1992). This research led to a more generic two-dimensional study of the noise generated by an air flow past two plates in tandem representing two successive teeth on a blade (Bull et al., 1996). The apparent shortage of experimental work showing a clear and straightforward agreement with theoretical prediction using Curle's equation led Bies et al. (1997) to use this arrangement to further investigate how Curle's equation applies in the case of a rigid body suspended in the vortex–wake of an upstream bluff body. Once again, the experimental results showed a discrepancy with the proposed theory. Sound power levels measured in a reverberation room were found to be up to 7 dB above the predictions based on the measured force acting on the downstream block, using Curle's equation and a compact source model. Extraneous contributions from the upstream blade were investigated by removing the radiating block. As a result, sound power levels decreased by more than 12 dB, which led to the conclusion that the upstream blade had a negligible acoustic contribution to the reference case under investigation and was not the cause for such a large under-prediction.

To account for the discrepancy between theory and experiment, Bies et al. (1997) suggested that the acoustic source was better represented by a superposition of a concentrated hydrodynamic force and an oscillating sphere (Morse, 1948), since the block was suspended on taut wires and vibrating. This explanation was later re-assessed (Leclercq, 2002) and the acoustic contribution from the body oscillations was demonstrated to be negligible in that case. Leclercq and Symes (2002) continued these investigations in a reverberation chamber, which consistently showed measured sound power levels up to 5 dB above those predicted using Curle's formulation.

Although practical in terms of providing a straightforward method of comparing experimental data with prediction, the use of a reverberation chamber limits the possibilities to investigate the nature of the sound field produced and to investigate particular noise contributions. Errors in sound power estimation may occur due to inconsistencies in the assumptions used to calculate sound power from sound pressure and the inclusion of additional noise, such as that from

fluctuating aerodynamic drag. A comprehensive discussion of some of the errors associated with reverberation chamber measurements for this type of flow can be found in Leclercq and Symes (2002).

To further investigate the possible reasons for the discrepancy observed in the reverberation chamber, an anechoic testing facility was built so that more advanced signal processing techniques could be implemented. Preliminary measurements (Leclercq and Symes, 2003) showed a significantly reduced discrepancy between the theoretical predictions and the measurements, and, in spite of a strong noise contribution from the untreated air supply, the two agreed within approximately 3 dB over the experimental range, after coherent output measurement techniques had been implemented. However small, this nonrandom discrepancy could not be clearly attributed to a given phenomenon, but was thought to be due to a phase relationship between the aerodynamic forces on each object that varied with flow speed. Discrepancies between Curle's theory and measurements continue to be used to support further questioning of the validity of Curle's theory (Bies, 2007), so it is important that these differences be resolved in order that Curle's theory be confirmed unambiguously.

This paper investigates the flow and noise generation associated with the interaction of a vortex–wake with a sharp edged bluff-body. The aim is to enhance the present level of understanding regarding these flows and to confirm, quantitatively, that the small difference observed between measurement and prediction using Curle's theory is indeed due to phase differences between the aerodynamic forces. Previous work (Johnson and Loehrke, 1984; Leclercq and Symes, 2003) only suppose that this is true without comparison of theoretical and experimental results.

The paper is organised as follows. After the Introduction (Section 1), Section 2 presents Curle's theory and a theoretical model of the noise generation process; Section 3 describes the experimental methods; Section 4 details the numerical techniques employed to calculate the aerodynamic flow field; Section 5 presents the aerodynamic results; Section 6 presents the acoustic results and their comparison with theory; the paper concludes in Section 7.

2. Theoretical development

2.1. Curle's theory

Following Lighthill's (1952) acoustic analogy formulation predicting the far-field noise generated by a finite region of turbulent flow, Curle (1955) proposed an extension to the case where rigid stationary boundaries were interacting with this flow. This theory and subsequent developments of the acoustic analogy have been extensively used since their publication to predict the noise generated by flows and their interaction with solid surfaces.

Curle's equation, when applied to the ideal simple case of a concentrated hydrodynamic force, simplifies to a degree such that the number of approximations can be significantly reduced when evaluating experimental results against theoretical or numerical predictions. Assuming a low subsonic flow, the sound radiated by a rigid, stationary body in a fluctuating flow can be written as the gradient of a surface pressure integral

$$4\pi c_0^2(\rho(\tilde{x},t)-\rho_0)=\frac{\partial}{\partial x_i}\int\int_S \frac{l_j}{r}[p\delta_{ij}]\,dS(\tilde{y}), \tag{1}$$

where c_0 and ρ_0 are the speed of sound and the fluid density in the medium at rest, respectively, and $\tilde{y}$ denotes a point on the rigid surface, separated from the observation point $\tilde{x}$ by the distance r. l_i are the components of the unit vector that is normal to the surface. The square brackets denote a value taken at the retarded time $t-r/c_0$.

When the integration is carried out on a surface of acoustically compact dimensions, Curle's equation can be simplified to predict the acoustic far-field generated at an observation point by a fluctuating point force $\tilde{F}$ applied on a compressible fluid that is initially at rest:

$$4\pi c_0^2(\rho(\tilde{x},t)-\rho_0)=-\frac{\partial}{\partial x_i}\left[\frac{F_i}{r}\right]=\frac{1}{c_0}\frac{x_i}{r^2}\left[\frac{\partial F_i}{\partial t}\right], \tag{2}$$

where F_i are the three vector components of the resulting force applied on the fluid. In the case of a harmonic force, $F_i(t)=\mathrm{Re}(F_i\,\mathrm{e}^{-\mathrm{i}\omega t})$ and

$$4\pi c_0^2(\rho(\tilde{x},t)-\rho_0)=-F_i\frac{\mathrm{i}\omega}{c_0}\frac{x_i}{r}\frac{\mathrm{e}^{-\mathrm{i}\omega(t-r/c_0)}}{r}, \tag{3}$$

which rearranges to the following expression for the complex radiated acoustic pressure ($\hat{p}$):

$$\hat{p}(\tilde{x},t)=-\mathrm{i}k_0F_i\frac{x_i}{r}\frac{\mathrm{e}^{-\mathrm{i}\omega(t-r/c_0)}}{4\pi r}. \tag{4}$$

Thanks to its simplicity, this basic formulation of Curle's equation has been evaluated against numerous experimental and numerical simulation results. Early work investigating the application of Curle's theory to the simple case of a concentrated dipole force led to discrepancies that were qualitatively attributed to spurious phenomena in the experimental set-up. Heller and Widnall (1970) studied the outlet noise generated by a turbulent flow around a spoiler located either inside a pipe, or just downstream of its exit plane. The noise level generated by the flow around the spoiler was found to be lower than that predicted using Curle's equation applied to the measured fluctuating forces acting on the airfoil. Heller and Windnall attributed this discrepancy to the influence of the nearby pipe outlet.

Clark and Ribner (1970) measured the cross-correlation between the resulting force applied to an acoustically compact airfoil located in the turbulent mixing region of a jet and the radiated acoustic pressure as well as the auto-correlation of the force. Comparing these functions at the value of the delay that corresponds to the maximum amplitude of the cross-correlation function, they deduced that the measured sound pressure was 73% of that predicted using Curle's equation with the measured force. They explained that this discrepancy was caused by a structural resonance in the airfoil mounting system that artificially increases the force measured by the piezo-electric transducer they use. This work, by the simplicity of its experimental arrangement, was at that time the most direct attempt at interpreting Curle's equation for the case of an acoustically compact body in a fluctuating flow.

Leehey and Hanson (1971) measured fluctuating lift forces and spanwise coherence length scales on cylinders in a cross-flow to verify Curle's equation. Their prediction agreed with their measurements within a tolerance of 3 dB. Extensive discussion on the use and validity of Curle's theory can be found in the texts by Goldstein (1976), Blake (1986), Crighton et al. (1992) and Howe (1998); the reader is referred to them for more detail.

Interestingly, Gloerfelt et al. (2005) showed that Curle's formulation could be re-cast as the diffraction of quadrupole source terms at the surface, thus illustrating the theoretical consistency of acoustic analogy methods. Inoue and Hatakeyama (2002) and Seo and Moon (2005) both performed direct numerical simulations of compressible cylinder flow and acoustic fields. Their results showed close agreement between simulation and the theory of Curle.

2.2. Theoretical model

As will be shown, experimental and numerical results reveal strong tonal spectra for both the measured force and sound levels. A theoretical noise model for aerodynamically interacting bodies is derived below that can be used to describe observed experimental and numerical behaviour. A harmonic force model is described first, which is subsequently used with the theory of Curle to develop expressions for far-field noise and the ratio of acoustic power between noise generated by the block and the total noise.

Fig. 1 is a schematic illustrating the vortex–wake interaction. A pair of objects is placed in a uniform stream of air with velocity U_∞, as shown. The thickness of each object is D and they are separated by a distance G. Vorticity is generated by the upstream object (labelled object 1) that is convected downstream with convection velocity U_c. This vorticity arrives at the downstream object (labelled object 2). Aerodynamic forces are generated on each object $(F_1(t), F_2(t))$ which in turn generate noise. It is assumed that, for the purposes of the theoretical model, a single harmonic force applies to each object, with identical frequency but different phase. The model can be extended so that harmonic forces at a multiple of frequencies can be considered, if desired.

2.2.1. Harmonic force model

It is assumed that the force generated by the upstream blade (F_1) is

$$F_1(t) = F_{1_0} \sin(\omega t) \tag{5}$$

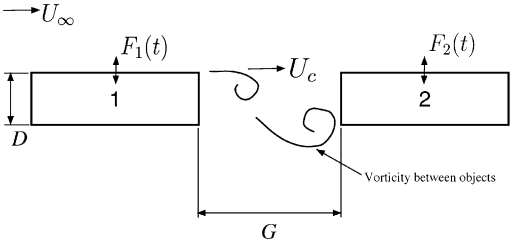

Fig. 1. Schematic illustrating the vortex–wake interaction.

and by the downstream block (F_2)

$$F_2(t) = F_{2_0} \sin(\omega t + \phi), \tag{6}$$

where ω is the vortex shedding frequency of the particular test. The Strouhal number is related to ω by

$$\mathrm{St} = \frac{\omega D}{2\pi U_\infty}.$$

The force developed by the downstream block emits sound at the same frequency as the upstream blade, but with phase difference ϕ. The phase shift varies with the distance between the blade and block (G). Determining what the phase difference is between the blade and block forces is not a trivial matter. It depends on the fluid mechanics of the particular configuration under study and whether a vortex–wake is established in the gap between the objects. For this work, the phase difference between the upstream and downstream unsteady lift forces is defined as

$$\phi = 2\pi \,\mathrm{St}\, \tau_0, \tag{7}$$

where τ_0 is the nondimensionalised time delay between the upstream and downstream lift forces as determined using a standard time-domain cross-correlation technique

$$\tau_0 = \frac{\Delta T U_\infty}{D}; \tag{8}$$

here, ΔT is the output from the cross-correlation analysis.

2.2.2. Noise model

Using the theory of Curle in its compact form, the sound due to a harmonic force developed by the upstream blade at observer position $\tilde{x} = [x_i]^{\mathrm{T}}$ is

$$p_1'(\tilde{x}, t) = \frac{1}{4\pi c_0} \frac{x_2}{r^2} (\omega F_{1_0}) \cos(\omega \tau), \tag{9}$$

where $\tau = t - r/c_0$ is the retarded time. The vertical component of the distance to the observer (x_2) is used as drag is neglected and only the lift is considered. In terms of the force on the downstream block, this sound becomes

$$p_1'(\tilde{x}, t) = \frac{1}{4\pi c_0} \frac{x_2}{r^2} (\omega B F_{2_0}) \cos(\omega \tau), \tag{10}$$

where $B = F_{1_0}/F_{2_0}$.

The sound radiated by the downstream block is

$$p_2'(\tilde{x}, t) = \frac{1}{4\pi c_0} \frac{x_2}{r^2} (\omega F_{2_0}) \cos(\omega \tau + \phi). \tag{11}$$

The combined sound is thus

$$p_c'(\tilde{x}, t) = \frac{1}{4\pi c_0} \frac{x_2}{r^2} (\omega F_{2_0}) [B \cos(\omega \tau) + \cos(\omega \tau + \phi)]. \tag{12}$$

The distance to the listener from each object is considered identical and acoustic path differences are neglected. This assumption is valid as long as the acoustic emitters are compact and in close proximity.

Using standard trigonometric identities, this reduces to the harmonic

$$p_c'(\tilde{x}, t) = \frac{1}{4\pi c_0} \frac{x_2}{r^2} (\omega F_{2_0}) \sqrt{1 + B^2 + 2B\cos\phi} \left[\cos\left\{ w\tau + \tan^{-1}\left(\frac{\sin\phi}{B + \cos\phi} \right) \right\} \right]. \tag{13}$$

It can be seen that Eq. (13) will reduce to Eq. (9) if $B \to \infty$ and Eq. (11) if $B \to 0$.

The power ratio

$$\mathrm{PR} = \left(\frac{\overline{p}_2'}{\overline{p}_c'} \right)^2 \tag{14}$$

is thus written in terms of the harmonic amplitudes,

$$\mathrm{PR} = \left(\frac{1}{\sqrt{1 + B^2 + 2B\cos\phi}} \right)^2. \tag{15}$$

Using the previously derived expression for phase (Eq. (7)), we have

$$\mathrm{PR} = \left[\frac{1}{\sqrt{1 + B^2 + 2B\cos\{(2\pi\,\mathrm{St}\,\tau_0)\}}}\right]^2. \tag{16}$$

This expression provides a convenient theoretical basis to understand the sound developed by two compact interacting bluff bodies. If a constant vortex convection velocity (U_c) is assumed, then the convection velocity can be determined from

$$U_c = \frac{G}{\Delta T}, \tag{17}$$

and the nondimensional time delay can be written as

$$\tau_0 = \frac{1}{k}\frac{G}{D}, \tag{18}$$

where $k = U_c/U_\infty$.

Fig. 2 plots the power ratio as calculated by Eq. (16) for $0 \leqslant B \leqslant 1.5$ over a blade–block separation range $3 \leqslant G/D \leqslant 10$ using the constant convection velocity assumption. For this calculation, it was assumed that $k = 0.7$ and $\mathrm{St} = 0.2$. When $B = 0$, all sound is produced by the downstream block and the power ratio is unity. As additional sound is introduced to the system via force oscillation on the upstream blade, the power ratio will vary with G/D. When $B < 1$, the power ratio oscillates about unity.

When $B = 1$, total cancellation of the two tones can occur and the power ratio becomes infinite at certain separation distances. This occurs when the separation distance is an odd multiple of one half the vortex–wake wavelength (λ_v), defined as the distance the shed vortices travel in one vortex shedding period. By inspecting the denominator of Eq. (16),

$$\left(\frac{G}{D}\right)_d\left(\frac{2\pi\,\mathrm{St}}{k}\right) = n\pi, \quad \left(\frac{G}{D}\right)_d = \frac{nk}{2\,\mathrm{St}} = \frac{n\lambda_v}{2D}, \tag{19}$$

where $\lambda_v = D(k/\mathrm{St})$, $(G/D)_d$ is the separation where destructive interference occurs and $n = 1, 3, 5, \ldots$.

As B becomes greater than unity, the power ratio becomes increasingly negative until as $B \to \infty$, $PR \to -\infty$.

Eq. (16) can be conveniently used to analyse the experimental results and assist with the comparison with predictions from the theory of Curle. The experiment measures both the force on the block and the combined sound pressure. Hence, a power ratio can be calculated using

$$\mathrm{PR} = \left(\frac{\overline{p}'_{2,\mathrm{Curle}}}{\overline{p}'_c}\right)^2, \tag{20}$$

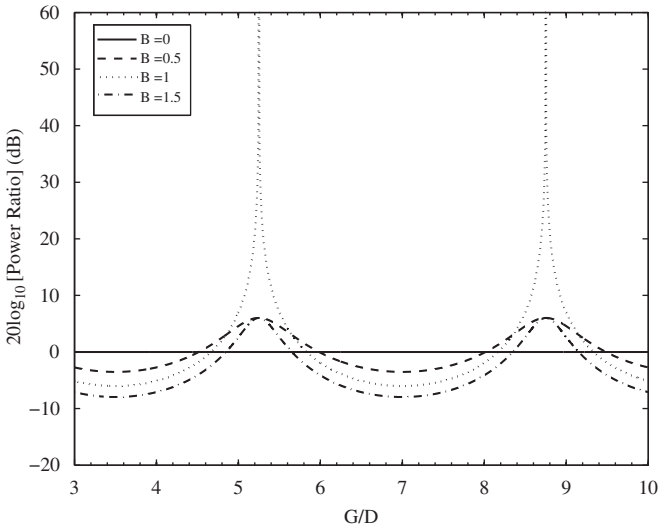

Fig. 2. Power ratio as calculated by Eq. (16) for $0 \leqslant B \leqslant 1.5$ over a blade–block separation range $3 \leqslant G/D \leqslant 10$. Constant convection velocity has been assumed with $k = 0.7$ and $\mathrm{St} = 0.2$.

where $\overline{p}'_{2,\mathrm{Curle}}$ is the root-mean-square (r.m.s.) sound pressure generated by the block as calculated by the theory of Curle using the experimentally measured force as an input to Eq. (2). As illustrated by the theoretical model, any variation in power ratio with separation distance is due to the amplitude ratio (B) and the phase difference (ϕ). In order to use the theoretical model to help explain experimental observations, experimental and numerical results are combined to provide meaningful estimates of B and ϕ.

3. Experimental arrangement

The case under investigation consists of a stationary rectangular solid block immersed in a fluctuating flow as sketched in Fig. 3. The interaction between the flow and the rigid surfaces results in acoustic noise generation, which is the phenomenon of interest. A vortex street is shed by an airfoil with an elliptical leading edge and a blunt trailing edge, referred to as a blade in this paper. The elliptical leading edge isolates vorticity production to the trailing edge. The blade is situated at the end of a $50 \times 50\,\mathrm{mm}^2$ duct, as shown in Fig. 3. The blade spans the duct completely and has a thickness $D = 8\,\mathrm{mm}$ and a chord length of 80 mm (or $10D$). The blade trailing edge is positioned one blade thickness upstream of the duct exit.

It is important to ensure that the blade does not excite an acoustic resonance within the duct in which it is situated. This was achieved by choosing a flow velocity so that the vortex shedding frequency of the blade was much lower than any duct mode resonance frequency. Following Parker (1967), the lowest resonance frequency is associated with the β mode and for the experimental conditions of the current work, the resonance Strouhal number should be $\mathrm{St}_\beta = 0.44$. As the maximum vortex shedding Strouhal number was found to be $\mathrm{St} = 0.2$, no acoustic duct modes are likely to be excited during this experiment.

The downstream block is a rectangular prism of chord 30 mm, span 30 mm with an identical thickness to the blade ($D = 8\,\mathrm{mm}$). The block is suspended on wires and has an embedded accelerometer for force measurement. Force is determined by multiplying the block mass by the measured acceleration. Calibration of the block mounted accelerometer was performed using an instrumented impact hammer. The calibration results showed that the block behaved as a mass in the frequency range of interest and that the flexibility of the suspending wires had negligible influence on force estimation. The block and the blade are separated by a distance G, which is varied from $3D$ to $6D$.

The fluid medium of interest is ambient air, of density ρ_0 in which the speed of sound is c_0. The experimental models were placed in an anechoic wind tunnel where the free-stream velocity (U_∞) was set to 44 m/s (Mach number $M_\infty = 0.13$) for all acoustic tests. The Reynolds number, based on model thickness was $\mathrm{Re}_D = U_\infty D/\nu = 35\,000$. A second series of experiments (Doolan and Leclercq, 2007) was also performed with the aim of investigating the velocity field about the upstream blade in isolation. These experiments were performed using a single component hot-wire with $U_\infty = 30\,\mathrm{m/s}$ and $\mathrm{Re}_D = U_\infty D/\nu = 24\,000$. Mean boundary layer heights and wake velocity profiles were obtained for

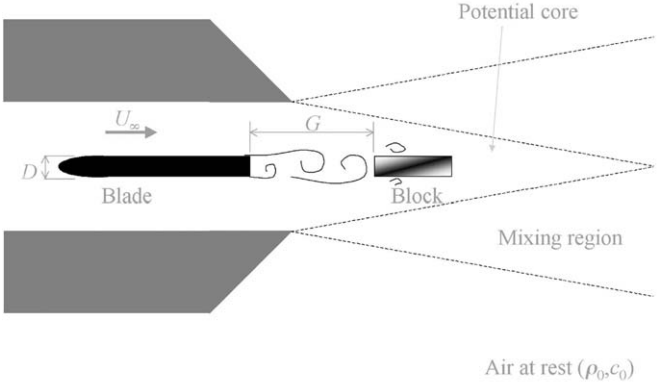

Fig. 3. Sketch of the test case and annotations.

comparison with numerical simulation. Additionally, hot-wire measurements showed that the boundary layer along the walls of the duct containing the blade was approximately 1.5 mm thick and the free-stream turbulence level was 0.37%.

The experimental apparatus was placed in an anechoic room. Two microphones were located on the axis of the expected dipole sound field, with a third microphone located at an angle of 60° from the axis. Two reference microphones were located in the plane of the block, where the dipole pressure field is ideally zero. These are therefore expected to measure the background noise. Using these carefully located reference sensors, the anechoic environment enabled the implementation of signal processing techniques to evaluate, and remove if necessary, the potential contribution from extraneous noise sources.

The flow speed of interest was kept in the low subsonic range ($M_\infty < 0.2$), so that the acoustic contribution from the flow itself, and convective effects on the acoustic field could be neglected (Roger, 1996). The frequency of the radiated tone was such that the length scale of the rigid body was much smaller than an acoustic wavelength.

It should be noted that the noise generation mechanism does not involve any acoustic feedback, as the tone Strouhal number does not present any discontinuity when plotted as a function of the flow velocity [consistent with Johnson and Loehrke (1984)]. The vortex-shedding phenomenon is well established on the blunt trailing edge of the blade, and is not triggered by acoustic waves emitted from the leading edge of the downstream block. There is, however, significant hydrodynamic feedback between the block and blade and this is observed through variations in both experimental and numerical Strouhal number results.

The simplified dipole formulation of Curle's equation applies to low Mach number flows for the case of acoustically compact material surfaces. If the dipole source is not acoustically compact, the full formulation of Curle's (1955) equation needs to be resolved to properly account for scattering by rigid surfaces. In the present experiment, the compact limit is approximately reached at a Strouhal number of 2. All results are presented below a Strouhal number of 0.5.

4. Numerical technique

4.1. Governing equations

To provide a better understanding of the flow about the blade and block, a computational model was developed based on the Unsteady Reynolds Averaged Navier–Stokes (URANS) and continuity equations:

$$\frac{\partial U_i}{\partial t} + U_j \frac{\partial U_i}{\partial x_j} = -\frac{\partial P}{\partial x_i} + \frac{\partial}{\partial x_j}(2\nu S_{ji} - \overline{u_j' u_i'}), \tag{21}$$

$$\frac{\partial U_i}{\partial x_i} = 0, \tag{22}$$

where $i,j = 1,2$ (two-dimensional), x is the position vector, P is the pressure, t is time and ν is the kinematic molecular viscosity. Further, the specific Reynolds-stress tensor is

$$\tau_{ij} = -\overline{u_j' u_i'} \tag{23}$$

and the strain-rate tensor is

$$S_{ij} = \frac{1}{2}\left(\frac{\partial U_i}{\partial x_j} + \frac{\partial U_j}{\partial x_i}\right). \tag{24}$$

The velocities (U_i) represented above are Reynolds averaged, hence the instantaneous velocity is $u_i = U_i + u_i'$ where u_i' is the fluctuating part of the velocity vector. Turbulence closure was provided by the standard two-equation $k-\varepsilon$ model (Launder and Sharma, 1974).

4.2. Numerical flow models

The development of the flow model was performed in two stages. The first stage involved the investigation of the flow about the upstream blade in isolation. The purpose of the development of this model was to test an assumption regarding the simplification of the flow domain for the blade. As upstream separation is suppressed using an elliptical leading edge, the main vorticity generation occurs at the trailing edge. Instead of simulating the complete flow about the blunt blade, a modified flow domain was used where only the flow over the trailing edge was considered. To obtain the

correct boundary layer height at the trailing edge, a flat plate boundary layer solution was used. The length of the flat plate is chosen to re-create the boundary layer height expected at the trailing edge of the blunt blade. The expected height of the blunt blade boundary layer is calculated using the empirical correlation of Brooks et al. (1989) for *untripped* boundary layers

$$\frac{\delta}{c} = 10^{[1.6569-0.9045\log\ \mathrm{Re}_c+0.0596(\log\ \mathrm{Re}_c)^2]}, \tag{25}$$

where δ is the boundary layer height, c is the chord of the original blade and Re_c is the Reynolds number based on the chord.

Using this empirical model and the standard turbulent boundary layer relations (Cebeci and Bradshaw, 1977), an effective length of flat plate can be used to re-create the same boundary layer height at the trailing edge. Using this method, it was determined that a flat plate of length $11.2D$ was required.

Therefore, the airfoil geometry is represented by a rectangle of length $11.2D$ and height D, where $D = 8$ mm. The flow domain is $28.7D \times 41D$ in the $x \times y$ directions, as shown in Fig. 4.

By developing the model about the upstream blade in isolation, critical parameters, such as mesh accuracy, mean boundary layer height and wake development could be assessed. Results of the simulations about the upstream blade are shown in Section 5.1 and illustrate the success of the flow domain simplification method.

Five meshes were used to establish the accuracy of the model about the blade in isolation. Details of each mesh are listed in Table 1 which lists the mesh density, maximum and average Δy_n^+ values adjacent to the walls of the trailing edge. The value Δy_n^+ is defined using (Wilcox, 2006)

$$\Delta y_n^+ = \sqrt{\frac{\tau_w}{\rho}}\frac{\Delta y_n}{\nu}, \tag{26}$$

where τ_w is the skin friction at the wall and Δy_n is the distance to the first grid point normal to the blade surface. These calculations were taken after the initial flow field transients had disappeared and at multiple time-steps. Wall functions are used in conjunction with a no-slip boundary condition at the walls.

Here, three methods, based on the Richardson extrapolation technique (Richardson, 1910), were used to estimate the accuracy of the solution. Three methods were required, as it is sometimes difficult to properly estimate the order of the solution, especially in turbulent flows (Celik and Karatekin, 1997; Roy, 2003).

The first- and second-order Richardson extrapolation methods of Celik and Karatekin (1997) were used. A special mixed-order technique (Roy, 2003) was also used. Including a mixed-order method was considered important because,

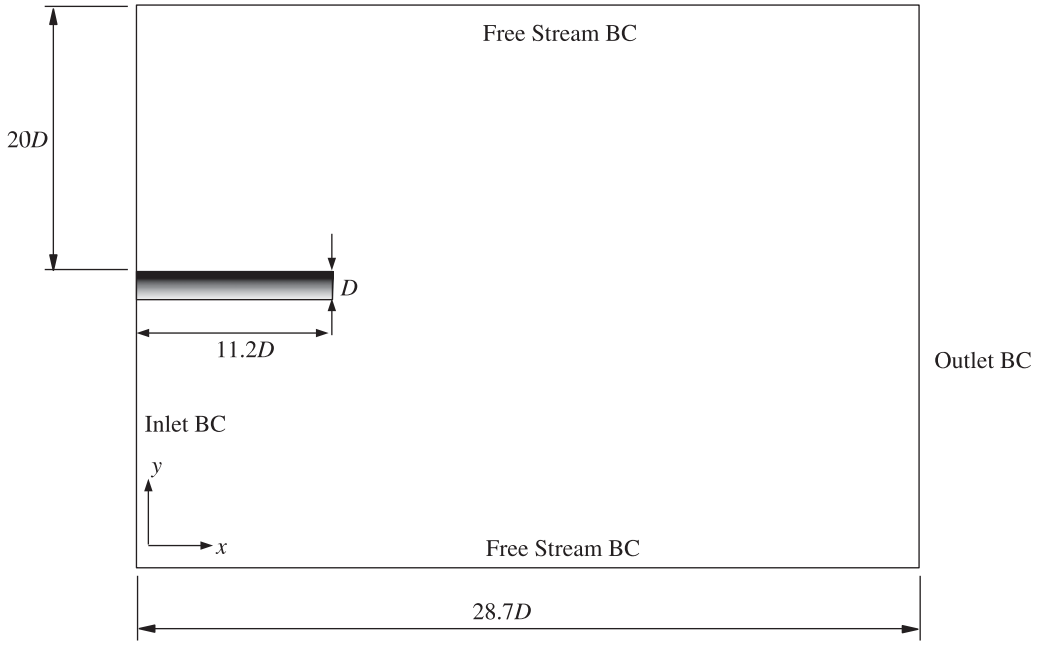

Fig. 4. Flow domain used for simulations about the upstream blade in isolation.

Table 1
Mesh density and Δy_n^+ values.

Mesh	$N_x \times N_y$	Maximum Δy_n^+	Average Δy_n^+
Very coarse	58×34	149.8	20.4
Coarse	115×65	102.4	17.5
Medium	163×91	80.9.4	15.2
Fine	230×130	56.4	12.2
Very fine	325×184	33.8	9.5

Table 2
Discretisation error results.

Order	Error, e_h (%)
Mixed order	2.34
First order	2.07
Second order	2.73

in the current flow simulations, the computational method was regarded as mixed and the order was expected to be realistically bounded between 1 and 2.

To estimate discretisation error, the time-varying flow velocity at a point $x = 1.75D, y = 0.75D$ from the trailing edge mid-plane was used for the analysis. Table 2 summarises the error calculated using the first-, second- and mixed-order schemes. It can be seen that the error of the solution was below 2.8% regardless of the order assumed.

The very fine mesh containing $N_x = 325 \times N_y = 184$ grid points was used for all simulations of the blade in isolation presented in this paper.

The second stage of model development involved constructing a series of computational meshes based on the very fine mesh of the above test case but including the downstream block. Careful construction of the mesh was performed for blade–block separation distances of $G/D = 1-6$ so that similar levels of mesh refinement were maintained in each case. For every mesh the downstream extent of the flow domain was kept at a constant distance from the trailing edge of the block ($17.5D$). The flow domain used for simulations involving the blade–block pair is shown in Fig. 5. Flow results for cases using this flow domain are presented in Section 5.2.

4.3. Computational details

The equations were discretised using a structured finite-volume method within the openFOAM software package (Jasak et al., 2004). The convective and diffusive terms were evaluated using a second-order accurate central-differencing method. Time integration was performed using an Euler method with the requirement that the maximum Courant number was kept below 0.2. The pressure-implicit split-operator (PISO) algorithm with two correction steps was used as an implicit, transient solution scheme. The resulting system of equations were solved using the incomplete Choleski conjugate gradient method with a solution tolerance of 10^{-6}.

4.4. Flow field initialisation

A two-dimensional potential flow solver is used to create a conservative flow field to initialise all simulations. Using this as the starting condition at $tU_\infty/D = 0$, the two-dimensional URANS equations are iteratively solved. It takes approximately 5000 time steps or a nondimensional time of 18.75 for vortex shedding to begin. All initial flow transients have disappeared by $tU_\infty/D = 150$ or 5.2 computational domain flow-through times.

Flow simulations are obtained after the initialisation period for $tU_\infty/D = 112.5$ nondimensional time units or four domain flow-through times. This corresponds to 30 000 time steps and captures 25 vortex shedding cycles with 1200 time steps per shedding period.

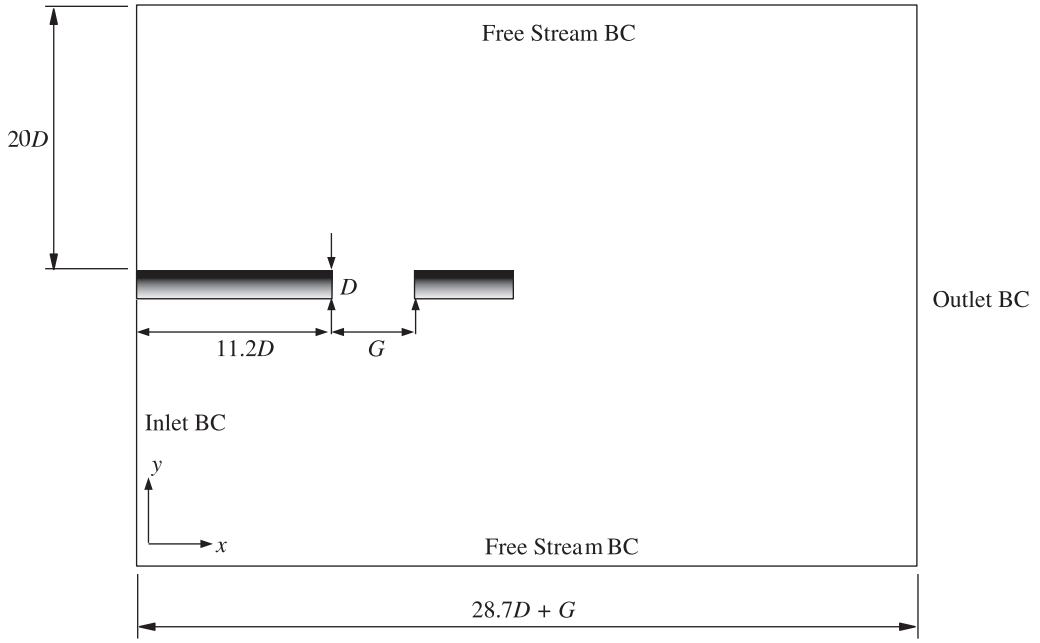

Fig. 5. Flow domain used for simulations about the blade–block pair.

Fig. 6. Contours of instantaneous vorticity magnitude at $tU_\infty/D = 262.5$ about the trailing edge region of the blade in isolation. The plot shows 50 equally spaced contours over a range of $0.67 < \omega D/U_\infty < 8$.

All numerical results were performed using a free-stream velocity of $U_\infty = 30\,\mathrm{m/s}$ corresponding to a Reynolds number based on the thickness of the blade D of $U_\infty D/\nu = 24\,000$.

5. Aerodynamic results

5.1. Blade in isolation

Contours of instantaneous vorticity magnitude calculated numerically are shown for the blade in isolation in Fig. 6. It can be seen that the numerical method successfully captures periodic vortex shedding from the trailing edge region and provides a description of the flow field behind the wake of the blade. Vortices are created at the trailing edge with an initially low convection velocity. These vortices are then accelerated downstream via the action of momentum transfer from the free stream to achieve an almost constant convection velocity.

Fig. 7(a) shows the unsteady lift and drag coefficients for the blade in isolation. The lift coefficient oscillates about a mean of zero with an amplitude of 0.183. The drag coefficient has a mean of 0.072 and a maximum value of 0.078. It can be noticed that the drag oscillates at approximately twice the frequency as the lift because each vortex shed from the blade causes the same change in drag but opposite changes in lift.

Fig. 7(b) shows the force power spectrum for the isolated blade, calculated using numerical data. The amplitude of the blade force is low and the Strouhal number is predicted to be 0.22, which is more than that measured experimentally by sound measurement methods (0.2). The over-prediction of shedding frequency is a common feature

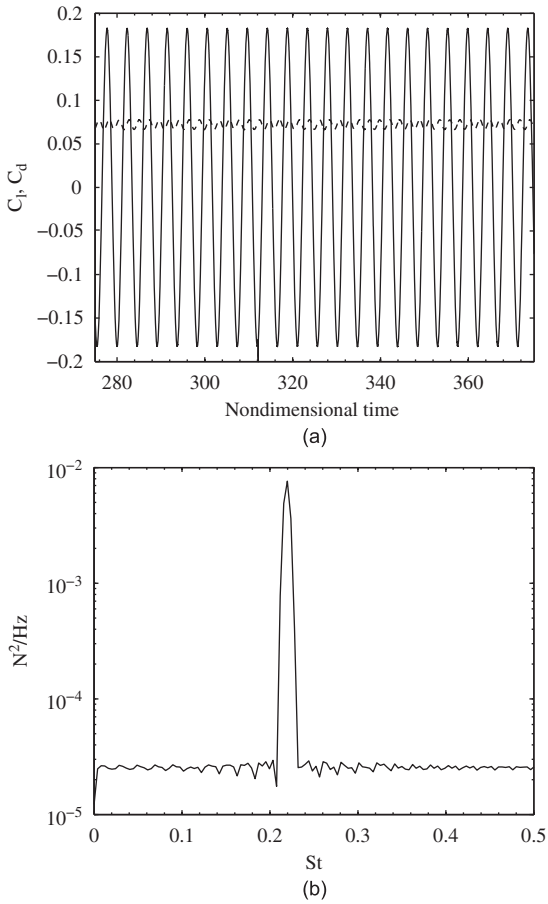

Fig. 7. Unsteady force numerical data for the blade in isolation. (a) Time signals. Numerical unsteady lift and drag coefficients. Solid line is lift, dashed line is drag. (b) Power spectrum of lift force calculated from numerical data.

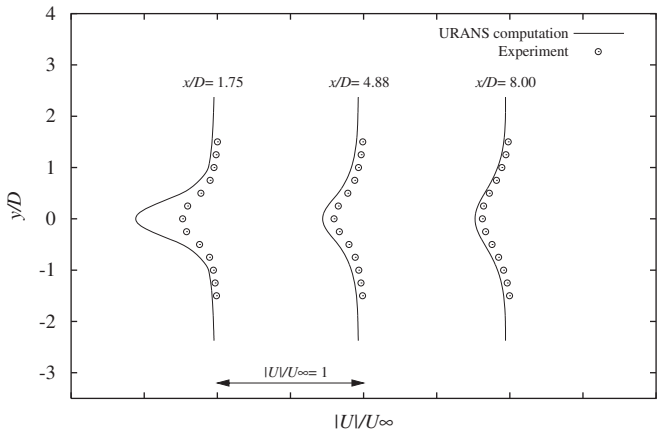

Fig. 8. Comparison between time averaged URANS computation and experiment at various wake cross-sections.

of two-dimensional URANS simulations [see for example Casalino et al. (2003)] and is mainly due to the over-prediction of Reynolds stresses in the near wake artificially constraining the size of the re-circulation bubble formed immediately behind the bluff body (Roshko, 1993).

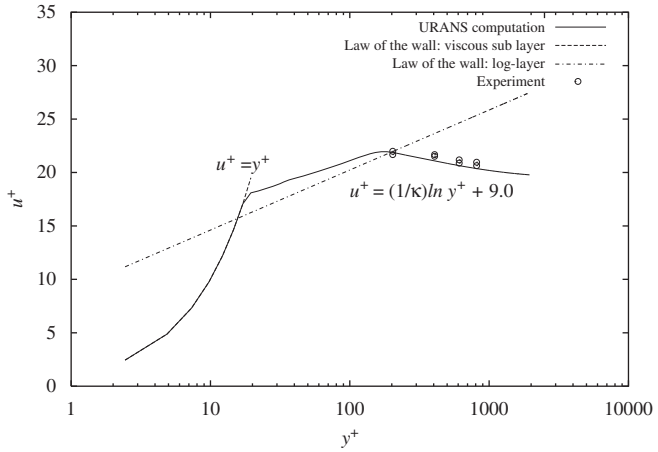

Fig. 9. Comparison between time averaged URANS computation, experiment and law of the wall.

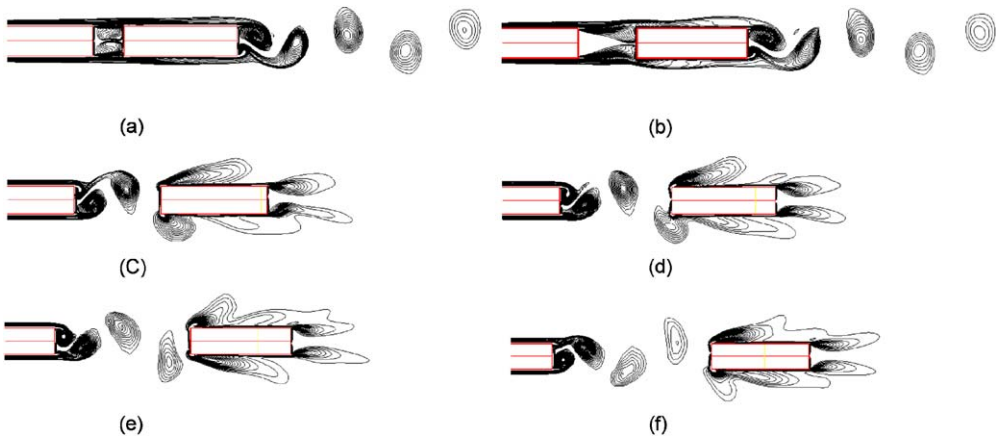

Fig. 10. Contours of instantaneous vorticity magnitude at $tU_\infty/D = 262.5$ for the vortex–wake interaction for (a–f) $G/D = 1-6$. Plot shows 50 equally spaced contours over a range of $0.67 < \omega D/U_\infty < 8$.

A comparison of mean wake numerical and experimental velocity data is shown in Fig. 8 and shows that the URANS computation poorly predicts the flow in the near wake, hence affecting vortex shedding frequency and recirculation bubble size, supporting previous arguments regarding the limitations of URANS simulations. However, further downstream, the comparison with experiment improves significantly.

Fig. 9 shows the mean streamwise velocity across the boundary layer region at the very end of the trailing edge. For these results, $y = y^+ = 0$ indicates the upper surface of the trailing edge and all results have been normalised using the friction velocity $u_\tau = \sqrt{\tau_w/\rho}$. Compared against the numerical results are the expected turbulent boundary layer profiles for the viscous sub-layer ($u^+ = y^+$) and the log-layer as assumed by the $k-\varepsilon$ turbulence model wall function ($u^+ = 1/\kappa \ln y^+ + C$). The intercept value used for the wall function was chosen to be $C = 9$ instead of the usual value of $C = 5$ for smooth walls. Comparison with single component hot-wire experimental data (Doolan and Leclercq, 2007) obtained at the edge of the defect-layer shows good agreement and gives confidence in the accuracy of the modelling assumptions used.

5.2. Wake–body interaction

5.2.1. Instantaneous flow field

Fig. 10 shows contours of instantaneous vorticity magnitude at identical times for numerical simulations with the blade and block pair at separation distance of $G/D = 1-6$. For $G/D < 3$ (Fig. 10(a, b)), vortex shedding is predominant

at the block trailing edge. The shear layers shed from the blade do not have an opportunity to form coherent vortex structures within the small gap. However, these shear layers, as well as the flow within the gap region, are unsteady. This behaviour has been observed experimentally (Bull et al., 1996) using hydrogen bubble visualisation in a water tunnel. Depending on Reynolds number, when $G/D \lesssim 3$, the flow is said to be in the 'trapped vortex' regime, with stable or quasi-stable vortices existing in the gap region and no vortex shedding by the upstream blade. The present numerical simulations successfully recreate this physical behaviour.

At $G/D \geqslant 3$ (Fig. 10(c–f)), the flow is said to *transition* (Bull et al., 1996) to the vortex shedding regime, where coherent vortex structures are now permitted within the gap region. After transition to the vortex shedding regime, impingement of vortex structures on the leading edge of the block occurs in a periodic fashion. The vortices then undergo a process of stretching caused by viscous effects at the surface of the block and the accelerating flow about the block.

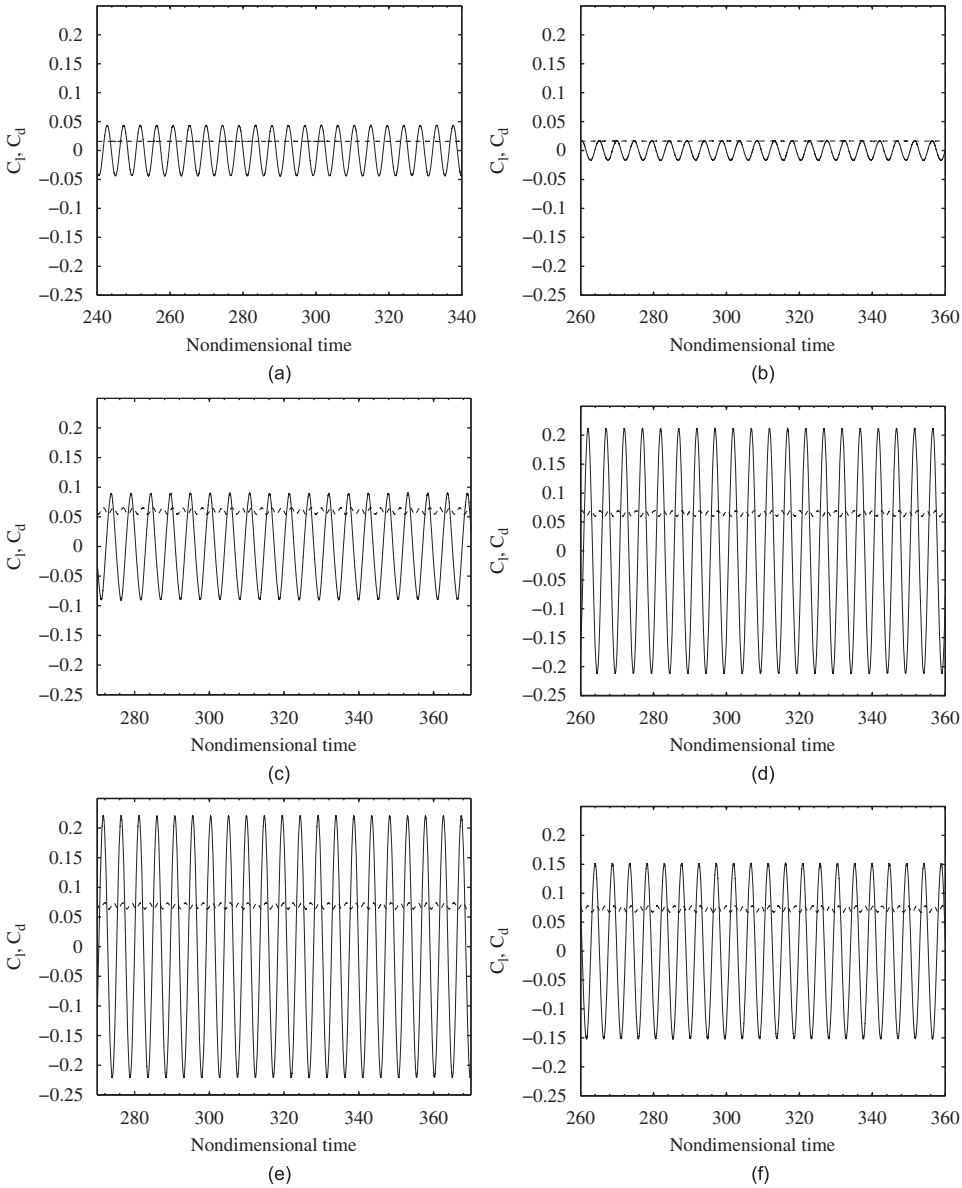

Fig. 11. Numerical unsteady lift and drag coefficients on the upstream blade for (a) $G/D = 1$; (b) $G/D = 2$; (c) $G/D = 3$; (d) $G/D = 4$; (e) $G/D = 5$; (f) $G/D = 6$.

As shown in Fig. 10(c–f), after impingement on the leading edge of the block, the vortex remains attached to the leading edge and is simultaneously stretched by the accelerating flow about the block. The flow velocity about the block was found numerically to be 20–23% higher than the free-stream velocity, causing acceleration of the vortex over the surface of the block. The stretching process dissipates the vortex and allows a weaker shed vortex system to form in the wake of the block.

It should be noted that this vortex acceleration process sets the rate of application of force to the block and affects the phase difference between the blade and block unsteady lift forces. It also shows that an assumption of constant vortex convection velocity is not valid for this type of flow.

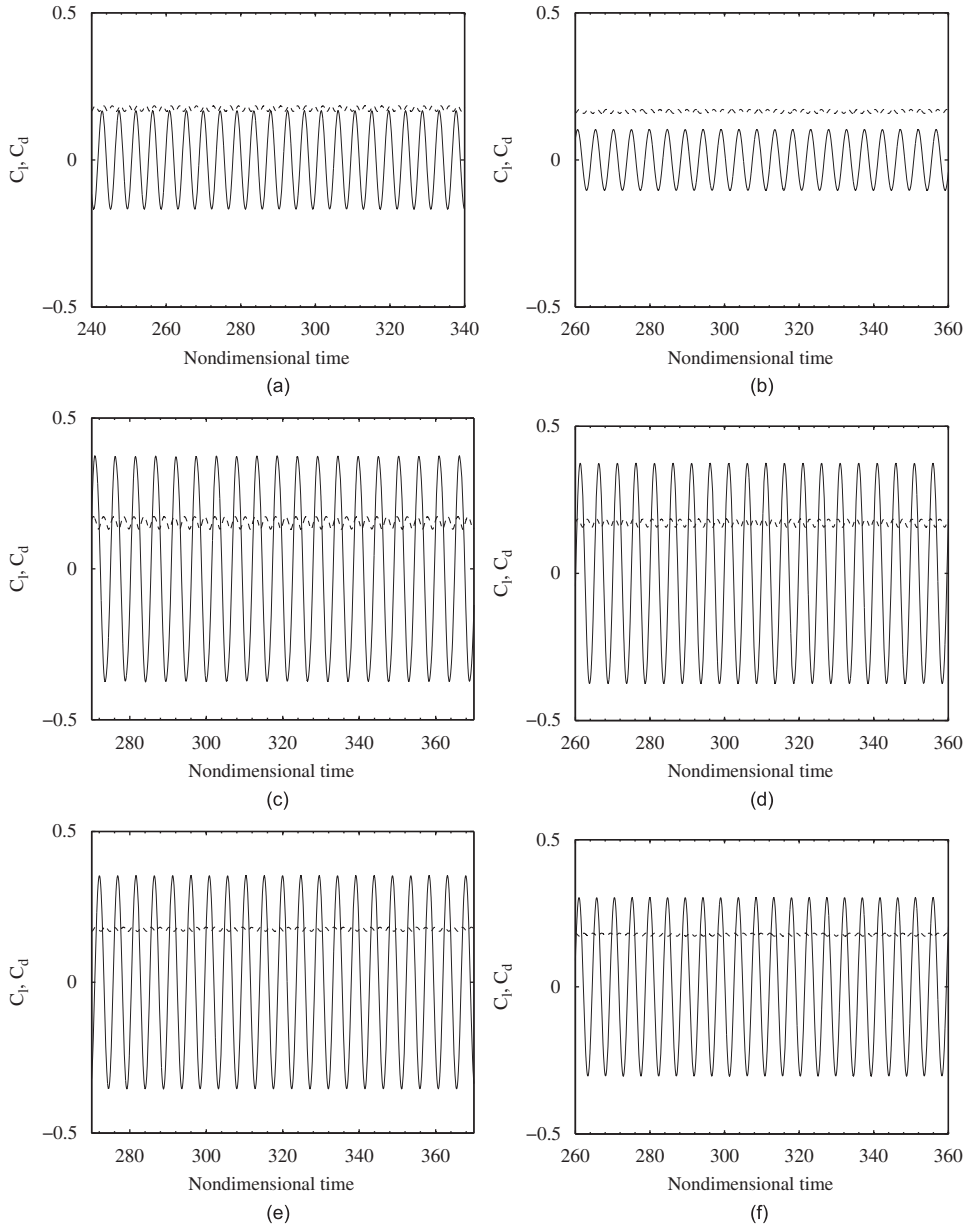

Fig. 12. Numerical unsteady lift and drag coefficients on the downstream block for (a) $G/D = 1$; (b) $G/D = 2$; (c) $G/D = 3$; (d) $G/D = 4$; (e) $G/D = 5$; (f) $G/D = 6$.

5.2.2. Unsteady forces

Fig. 11 shows the numerical unsteady lift and drag coefficients for the upstream blade for separation distances of $G/D = 1-6$. These forces, particularly the lift force, vary dramatically depending on separation distance.

The unsteady forces developed on the block for each G/D ratio are displayed in Fig. 12 as lift and drag coefficients. In the trapped vortex regime (Fig. 12(a, b)), the drag reduces slightly as G/D increases and the amplitude of the lift reduces by a much greater amount. The reduction in lift amplitude is due to the upstream shear layer becoming unstable, disturbing the boundary layers on the block and reducing the magnitude of the vorticity shed at the trailing edge.

Once transition to the vortex shedding regime has occurred (Fig. 12(c–f)), the amplitude of the fluctuating lift coefficient increases greatly due to the forces developed by vortex impingement on the leading edge. Hence, the interaction of the upstream vortex with the block surface induces forces that are higher than those developed by vortex shedding alone.

The r.m.s. numerical lift coefficients for the blade and block are compared in Fig. 13. In all cases, the r.m.s lift coefficient calculated for the downstream block is higher than the upstream blade. Also, the r.m.s. lift coefficient increases on both objects as the vortex shedding mode is established at $G/D \geqslant 3$. However, while the block r.m.s. lift coefficient peaks at $G/D = 3$, the r.m.s. lift coefficient of the blade increases until $G/D \approx 5$.

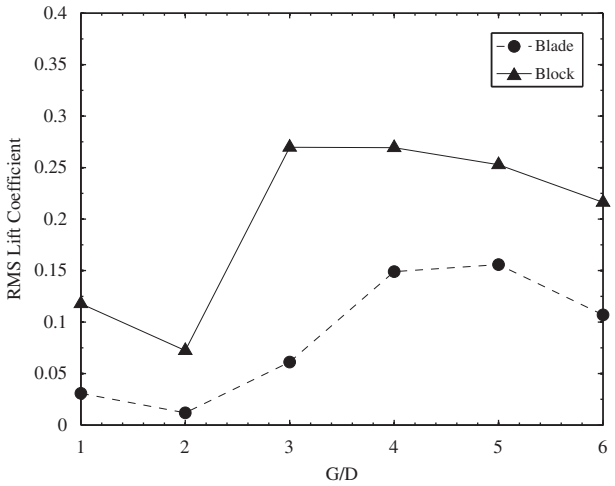

Fig. 13. Numerical r.m.s. lift coefficients for the blade and block over $G/D = 1-6$.

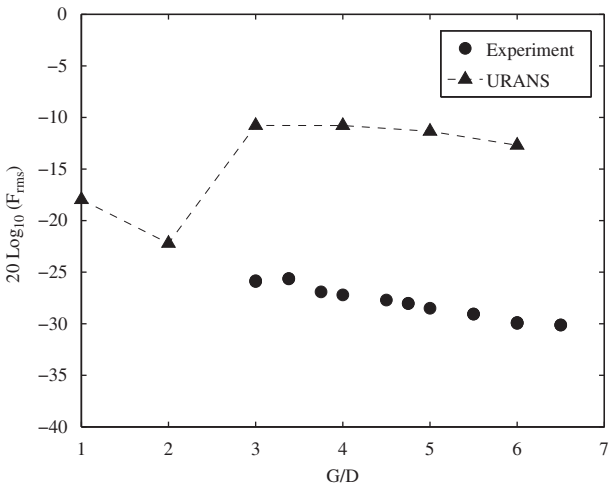

Fig. 14. Comparison of experimental and numerical r.m.s. lift for $G/D = 1-6$.

Fig. 14 compares the root-mean-square force (F_{rms}) applied on the block as a result of its interaction with the flow with its numerical counterpart, which were calculated using the planform area of the block used in the experiments. The experiments were only performed in the vortex shedding regime with $G/D \geqslant 3$. Hence the experimental results show a monotonic decrease in F_{rms} with increasing G/D, due to increasing diffusion of the vortex over increasing gap lengths. Numerical results show the same trend as the experiments, but do not show as rapid a decrease in F_{rms} implying less turbulent diffusion. This is to be expected as the simulations did not allow streamwise vorticity to develop (as they were two-dimensional).

A striking feature of Fig. 14 is the differences in magnitude between numerical and experimental data. This can be attributed to three-dimensional flow about the block in the experiment. This will result in the development of streamwise vorticity (pressure release) that is not captured in the simulations. Fig. 14 therefore gives a useful estimate for the order of correction required when performing two-dimensional simulations of this nature.

Fig. 15 shows the variation in force amplitude ratio B with separation distance calculated using the numerical data. The force amplitude is not simply the ratio of lift coefficients, as the planform areas of the blade (4000 mm^2) and block (900 mm^2) are significantly different. The amplitude ratio is approximately unity until transition to the vortex shedding regime occurs. When $G/D > 3$, the force on the upstream blade becomes approximately 2.5 times higher. Hence, the blade would be expected to produce more acoustic energy than the downstream block. However, as will be shown, this is not observed during the experiment and it is believed that this effect is due to three-dimensional flow not taken into consideration in the simulations. As the blade is positioned at the end of a duct, the pressure constraining effect of the end-walls is removed just downstream of the blade trailing edge. This allows some near wake streamwise vorticity to develop that reduces the effective unsteady lift (and noise) amplitude.

Table 3 compares experimental and numerical Strouhal numbers for $G/D \geqslant 3$. In all compared cases, numerical calculations predict a vortex shedding frequency that is higher than experiment. As mentioned earlier, this is due to an over-prediction of in-plane Reynolds stresses in the near wake.

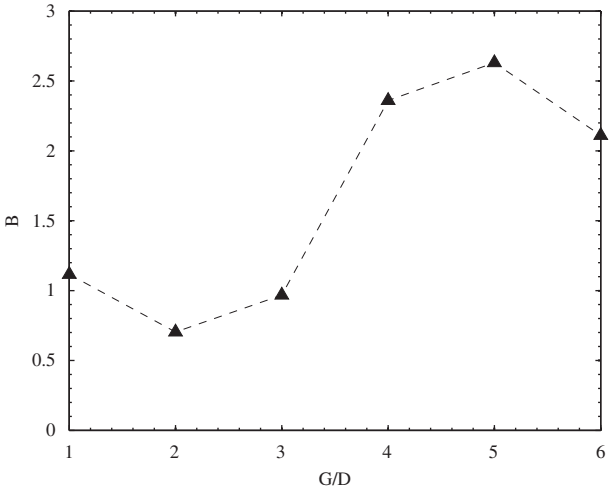

Fig. 15. Amplitude ratio, $B = F_{1_0}/F_{2_0}$, computed using numerical data.

Table 3
Strouhal number, time-delay, phase and amplitude ratio.

G/D	St (experiment)	St (numerical)	τ_0	ϕ (rad)	B
1	–	0.221	–	–	1.116
2	–	0.207	–	–	0.703
3	0.164	0.187	2.70	1.01π	0.968
4	0.184	0.200	5.67	2.27π	2.360
5	0.191	0.207	6.38	2.64π	2.631
6	0.196	0.213	8.16	3.48π	2.111

Table 3 also lists the nondimensional time delay τ_0 for $G/D \geqslant 3$. This value was calculated from the numerical results using a cross-correlation time-delay method where the force on each component was used in the analysis. Using this time delay and Strouhal number, the phase difference ϕ could also be determined. The phase is seen to vary from 1.01π to 3.48π depending on separation distance. Therefore, based on the theoretical model presented in Section 2.2, the noise level can be expected to be reduced when $G/D \approx 3$ due to the favourable phase relationship (i.e. $\phi \approx \pi$). As the separation distance is increased, the noise level will be expected to increase until $G/D \approx 3.7$ as the phase difference approaches 2π. Noise will be reduced again as separation distance is increased to $G/D \approx 5.5$ when $\phi \approx 3\pi$. This cycle of noise cancellation and reinforcement can be expected to continue as G/D is increased. The numerically calculated amplitude ratio B is also listed in the table for completeness.

6. Acoustic results

6.1. Noise from the blade in isolation

The noise power spectrum measured at microphone 1 for the case of the blade operating in isolation is shown in Fig. 16(a). In Fig. 16(b) the noise calculated using numerical force data and Curle's theory is presented. The numerical data has been shifted in frequency so that the main tone occurs at an identical Strouhal number to the experiment. According to Curle's theory (Eq. (3)), linear frequency scaling also necessitates a small scaling in amplitude. The frequency and amplitude were scaled according to

$$f_{\text{shift}} = f\frac{\text{St}_{\text{exp}}}{\text{St}_{\text{num}}}, \tag{27}$$

$$\Delta\text{SPL(dB)} = 20\log_{10}\frac{\text{St}_{\text{exp}}}{\text{St}_{\text{num}}}. \tag{28}$$

The numerical sound level is much greater than what is measured in experiment at frequencies about the tone. The ratio of experimental to numerical r.m.s. sound pressure was found to be 0.0113. It is assumed that this is due to three-dimensional flow effects as explained earlier, and possibly shielding of the noise due to the duct walls. This same scaling factor is applied to the numerical force data for comparison purposes with experiment (the empirical correction of B).

6.2. Noise measurements for the vortex–wake interaction

Fig. 17 shows the pressure power spectral densities measured at microphone 1 with $G/D = 3-6$ and without the block ($G/D = \infty$), at a flow speed of 44 m/s. The peaks are sharp and well defined at more than 20 dB above background noise levels. The figure also shows that when the block is removed, the blade alone emits a tone that is 17–21 dB below the tone emitted by the block, depending on the value of G/D. The measured acoustic power was found to vary with blade–block separation distance in the experiment. The theoretical model can be used with numerically computed values to explain this observed discrepancy and improve understanding regarding the physics of the noise generation mechanism.

Fig. 18 shows the pressure power spectral density as measured by microphone M1 (which is placed directly above the experiment in the plane of the dipole acoustic field), the coherent output power with reference to the block accelerometer, and that predicted from the measured block acceleration for $G/D = 6$ using the theory of Curle. This figure shows that the dominant contribution to the radiated tone is a source that is coherent with the force applied on the block. It also allows the reader to estimate the difference between the (unfiltered) measured signal and the coherent one.

At higher frequencies ($\text{St} > 0.25$), the measured signal is larger than the coherent one. The coherent signal is obtained by finding the cross-spectral density between the block acceleration and the noise signals. It is essentially a filtering technique that rejects components of the noise signal that are not coherent with the force on the block. As shown in Fig. 18, there are high frequency, noncoherent components of noise in the experiment, and these can be attributed to flow turbulence and other broadband sources. At higher frequencies, the predicted noise signal is at the same level as the measured one and indicates that the incoherent noise in the block acceleration signal is of the same magnitude as the incoherent noise developed by turbulence and other sources.

As shown in Section 2.2, the noise radiated by the blade cannot be removed from the measured noise signals. Based on experimental measurements, if the noise emitted by the blade were not affected by the presence of the block, this would lead to an expected discrepancy of up to 1.3 dB between the noise as predicted from the block vibration and the measured acoustic pressure. However, this is not the case, as illustrated by the data points in Fig. 19. These points

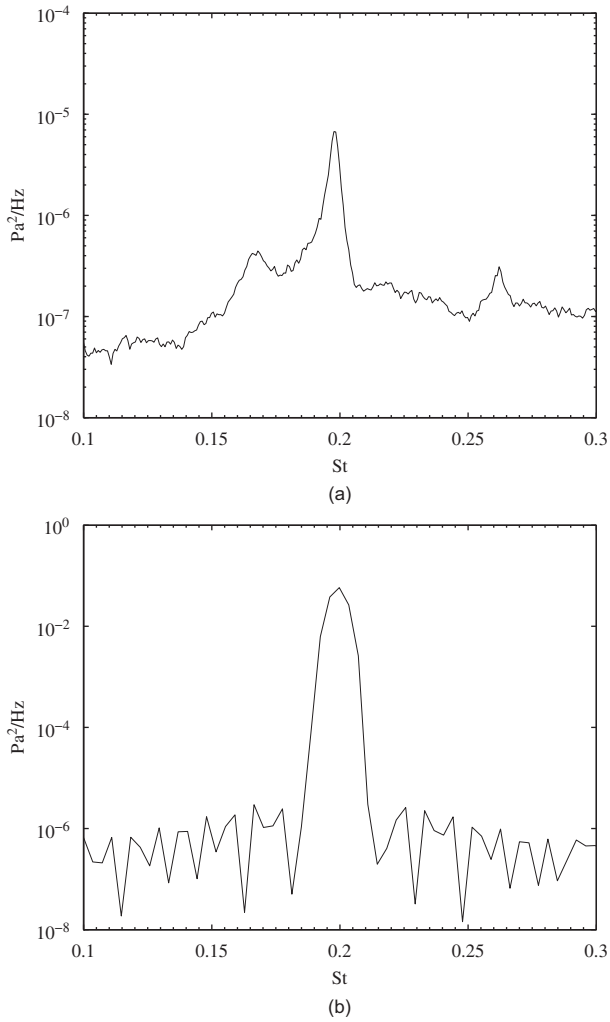

Fig. 16. (a) Experimental noise power spectrum for blade in isolation. (b) Noise power spectrum calculated from numerical data.

are the power ratio as calculated by Eq. (20) using experimental force and noise measurements. The power ratio clearly shows an oscillating behaviour as a function of G/D.

Fig. 19 also shows the power ratio as calculated using the theoretical model in the form of Eq. (15). In order to use Eq. (15), accurate values of amplitude ratio (B) and phase (ϕ) need to be obtained. In this work, numerical values of amplitude ratio are used; however, they are modified in two ways in order to be consistent with the experimental results. First, the scaling factor obtained in Section 6.1 is used to take into account the difference between numerical and experimental unsteady force on the upstream blade. Second, the difference between measured and computed force on the downstream block is accounted for by using scaling factors derived from the results in Section 5.2.2. The numerical values of phase are used (Table 3) without modification. As numerical simulations were performed at limited values of G/D, values of B and ϕ at intermediate points were estimated using an interpolation method based on a cubic spline.

As shown in Fig. 19, the comparison between theory and experiment is, overall, very good and shows that the phase relationship as described by the numerical analysis is accurate over most of the experimental range. Given the correct phase and amplitude relationship (as defined by the aerodynamic interaction), Curle's theory shows how the acoustic radiation from two compact bodies can cancel or reinforce each other depending on their separation distance. These results give increased confidence in the use of Curle's theory for predicting the noise emitted from acoustically compact aerodynamically interacting bodies. It also shows that the analytical theory derived in this paper is a valid means for describing the physics of noise generation for this particular aeroacoustic application.

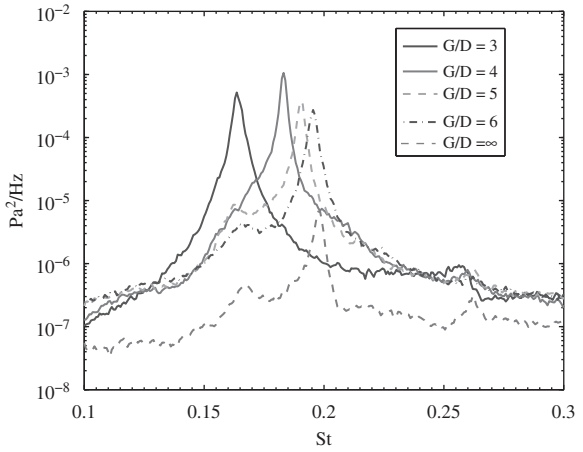

Fig. 17. Measured sound power spectral density at Mic. 1 measured for various values of G/D.

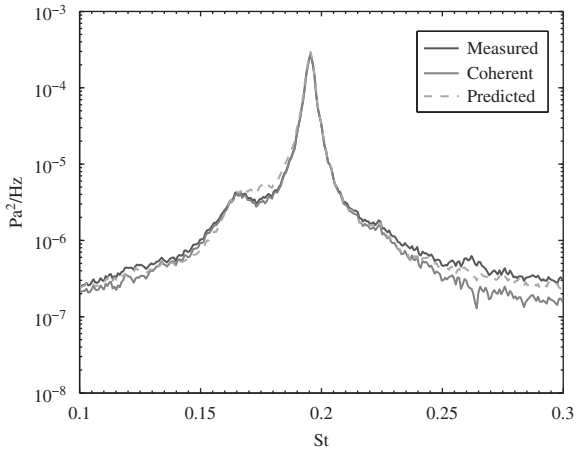

Fig. 18. Measured sound power spectral density at Mic. 1, $G/D = 6$.

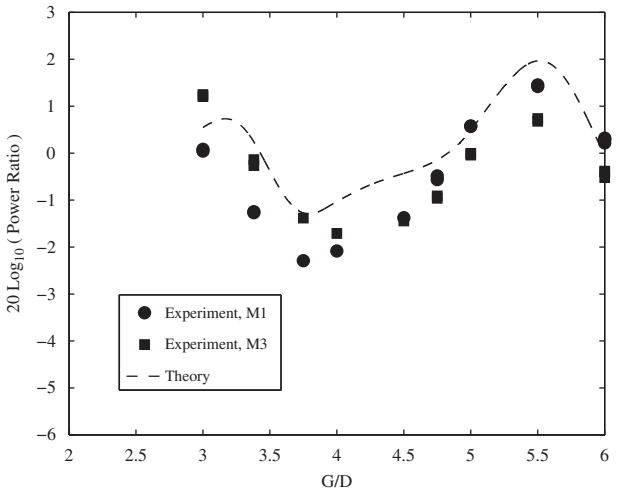

Fig. 19. Measured and predicted power ratio.

7. Conclusion

The force and noise generated by the interaction of a vortex–wake with a prismatic bluff body (or block) has been investigated. A theoretical noise model, based on the theory of Curle in its compact form, was developed and successfully used to explain observed discrepancies in acoustic measurements. The model shows how unsteady force amplitude and phase difference affect noise in the far-field. Experimental and unsteady numerical simulations were used to obtain these parameters as a function of the separation distance between the blade and block. Two-dimensional numerical simulation results were able to accurately predict the phase relationship between the unsteady lift forces developed on the blade and block. Physically, the phase difference was found to be controlled by the aerodynamic interference developed when an object is placed in the wake of the vortex generator.

The present results leave little room to question the accuracy and performance of Curle's fundamental theoretical work in the present case. This is in contrast to what has been suggested by Zinoviev and Bies (2004) and Bies (2007) based on earlier experimental results published by Bies et al. (1997).

Acknowledgements

This work was supported by a Large Grant from the Australian Research Council. Computing resources were made available by the South Australian Partnership for Advanced Computing. The authors would also like to thank the reviewers for their detailed and insightful comments that have made this a much better paper.

Research undertaken for this paper has been assisted with a grant from the Sir Ross and Sir Keith Smith Fund (Smith Fund) (www.smithfund.org.au). The support is acknowledged and greatly appreciated. The Smith Fund by providing funding for this project does not verify the accuracy of any findings or any representations contained in it. Any reliance on the findings in any written report or information provided should be based solely on the reader's own assessment and conclusions. The Smith fund does not accept any responsibility or liability from any person, company or entity that may have relied on any written report or representations contained in this report if that person, company or entity suffers any loss (financial or otherwise) as a result.

References

Bies, D., 2007. A review of selected experiments. Investigation of Curle's theory. In: Proceedings of the 14th International Congress on Sound and Vibration, Cairns, Australia.

Bies, D., Pickles, J., Leclercq, D., 1997. Aerodynamic noise generation by a stationary body in a turbulent air stream. Journal of Sound and Vibration 204 (4), 631–643.

Blake, W.K., 1986. Mechanics of Flow-induced Sound and Vibration, vol. 2. Academic Press, New York.

Blazewicz, A., Bull, M., Kelso, R., 2007. Characteristics of flow regimes for two plates of rectangular cross-section in tandem. In: Jacobs, P. (Ed.), Proceedings of the 16th Australasian Fluid Mechanics Conference, vol. 930–934.

Brooks, T., Pope, D., Marcolini, M., 1989. Airfoil self-noise and prediction. Reference Publication 1218, NASA, July.

Bull, M., Blazewicz, A., Pickles, J., Bies, D., 1996. Interaction between a vortex–wake and an immersed rectangular plate. Experimental Thermal and Fluid Science 12, 209–220.

Casalino, D., Jacob, M., Roger, M., 2003. Prediction of rod-airfoil interaction noise using the fw-h analogy. AIAA Journal 41 (2), 182–191.

Cebeci, T., Bradshaw, P., 1977. Momentum Transfer in Boundary Layers. McGraw-Hill, New York.

Celik, I., Karatekin, O., 1997. Numerical experiments on application of richardson extrapolation with nonuniform grids. ASME Journal of Fluids Engineering 119, 584–590.

Clark, P., Ribner, H., 1970. Direct correlation of fluctuating lift with radiated sound for an airfoil in turbulent flow. Journal of the Acoustical Society of America 46 (3), 802–805.

Crighton, D., Dowling, A., Williams, J.F., Heckl, M., Leppington, F., 1992. Modern Methods in Analytical Acoustics. Lecture Notes. Springer, London.

Curle, N., 1955. The influence of solid boundaries on aerodynamic sound. Proceedings of the Royal Society of London A 231, 505–514.

Devarakonda, R., Humphrey, J., 1996. Experimental study of turbulent flow in the near wakes of single and tandem prisms. International Journal of Heat and Fluid Flow 17, 219–227.

Doolan, C., Leclercq, D., 2007. An anechoic wind tunnel for the investigation of the main-rotor/tail-rotor blade vortex interaction. In: Proceedings of the Sixth Australian Vertiflite Conference on Helicopter Technology, March 2007. American Helicopter Society International, Inc.

Fitzpatrick, J.A., 2003. Flow/acoustic interactions of two cylinders in cross-flow. Journal of Fluids and Structures 17, 97–113.

Gloerfelt, X., Pérot, F., Bailly, C., Juvé, D., 2005. Flow-induced cylinder noise formulated as a diffraction problem for low Mach numbers. Journal of Sound and Vibration 287, 129–151.

Goldstein, M., 1976. Aeroacoustics. McGraw-Hill, New York.
Hangan, H., Vickery, B., 1999. Buffeting of two-dimensional bluff bodies. Journal of Wind Engineering and Industrial Aerodynamics 82, 173–187.
Havel, B., Hangan, H., Martinuzzi, R., 2001. Buffeting for 2d and 3d sharp-edged bluff bodies. Journal of Wind Engineering and Industrial Aerodynamics 89, 1369–1381.
Heller, H., Widnall, S., 1970. Sound radiation from rigid flow spoilers correlated with fluctuating forces. Journal of the Acoustical Society of America 47 (3), 924–936.
Howe, M., 1998. Acoustics of Fluid–structure Interactions. Cambridge University Press, Cambridge, UK.
Inoue, O., Hatakeyama, N., 2002. Sound generation by a two-dimensional circular cylinder in a uniform flow. Journal of Fluid Mechanics 471, 285–314.
Jacob, M.C., Boudet, J., Casalino, D., Michard, M., 2005. A rod-airfoil experiment as a benchmark for broadband noise modeling. Theoretical and Computational Fluid Dynamics 19, 171–196.
Jasak, H., Weller, H., Nordin, N., 2004. In-cylinder cfd simulation using a C++ object orientated toolkit. Technical Report SAE Technical Paper 2004-01-0110, Society of Automotive Engineers.
Johnson, C., Loehrke, R., 1984. An experimental investigation of wake edge tones. AIAA Journal 22 (9), 1249–1253.
Khorrami, M.R., Choudhari, M.M., Lockard, D.P., Jenkins, L.N., McGinley, C.B., 2007. Unsteady flowfield around tandem cylinders as prototype component interaction in airframe noise. AIAA Journal 45 (8), 1930–1941.
Launder, B., Sharma, B., 1974. Application of the energy dissipation model of turbulence to the calculation of flow near a spinning disc. Letters in Heat and Mass Transfer 1 (2), 131–138.
Leclercq, D., 2002. Comments on "Aerodynamic noise generation by a stationary body in a turbulent air stream". Journal of Sound and Vibration 260 (1), 183–190.
Leclercq, D., Symes, M., 2002. Dense compact rigid object in a turbulent flow: application of Curle's theory. In: Eighth AIAA/CEAS Aeroacoustics Conference, Breckenridge, USA, No. AIAA-2002-2577.
Leclercq, D., Symes, M., 2003. Curle's theory and implications for dense acoustically compact objects in turbulent flows. In: Ninth AIAA/CEAS Aeroacoustics Conference, Hilton Head, USA, No. AIAA-2002-3231.
Leehey, P., Hanson, C., 1971. Aeolian tones associated with resonant vibration. Journal of Sound and Vibration 13, 465–483.
Lighthill, M., 1952. On sound generated aerodynamically: general theory. Proceedings of the Royal Society of London A 221, 564–587.
Martin, B., Bies, D., 1992. On aerodynamic noise generation from vortex shedding in rotating blades. Journal of Sound and Vibration 155 (2), 317–324.
Meneghini, J.R., Saltara, F., Siqueira, C., Ferrari, J., 2001. Numerical simulation of flow interference between two circular cylinders in tandem and side-by-side arrangements. Journal of Fluids and Structures 15, 327–350.
Morse, P., 1948. Vibration and Sound, second ed. McGraw-Hill, New York.
Obi, S., Tokai, N., 2006. The pressure–velocity correlation in oscillatory turbulent flow between a pair of bluff bodies. International Journal of Heat and Fluid Flow 27, 768–776.
Papaioannou, G.V., Yue, D., Triantafyllou, M., Karniadakis, G., 2006. Three-dimensionality effects in flow around two tandem cylinders. Journal of Fluid Mechanics 558, 387–413.
Parker, R., 1967. Resonance effects in wake shedding from parallel plates: calculation of resonant frequencies. Journal of Sound and Vibration 5 (2), 330–343.
Richardson, L., 1910. The approximate arithmetic solution by finite differences of physical problems involving differential equations with application to stresses in a masonry dam. Transactions of the Royal Society of London, Series A 210, 307–357.
Roger, M., 1996. Fundamentals of Aero-acoustics, Part I. Lecture Series 1996-04, Von Karman Institute for Fluid Dynamics.
Roshko, A., 1993. Perspectives on bluff body aerodynamics. Journal of Wind Engineering and Industrial Aerodynamics 49, 79–100.
Roy, C., 2003. Grid convergence error analysis for mixed-order numerical schemes. AIAA Journal 41 (4), 595–604.
Seo, J.-H., Moon, Y.J., 2005. Perturbed compressible equations for aeroacoustic noise prediction at low Mach numbers. AIAA Journal 43 (8), 9.
Stoneman, S., Hourigan, K., Stokes, A., Welsch, M., 1988. Resonant sound caused by flow past two plates in tandem in a duct. Journal of Fluid Mechanics 192, 455–484.
Wilcox, D., 2006. Turbulence Modeling for CFD, third ed. DCW Industries, La Canada, CA, USA.
Zdravkovich, M., 1987. Review of flow interference between two circular cylinders in various arrangements. ASME Journal of Fluids Engineering 99, 618–631.
Zinoviev, A., Bies, D., 2004. On acoustic radiation by a rigid object in a fluid flow. Journal of Sound and Vibration 269, 535–548.